New calculations of gross β-decay properties for astrophysical applications: Speeding-up the classical *r* process

Peter Möller
Theoretical Division, Los Alamos National Laboratory, Los Alamos, New Mexico 87545

Bernd Pfeiffer and Karl-Ludwig Kratz
Institut für Kernchemie, Universität Mainz, Germany

(Received 30 May 2002; revised manuscript received 15 January 2003; published 19 May 2003)

Recent compilations of experimental gross β-decay properties, i.e., half-lives ($T_{1/2}$) and neutron-emission probabilities (P_n), are compared to improved global macroscopic-microscopic model predictions. The model combines calculations within the quasiparticle (QP) random-phase approximation for the Gamow-Teller (GT) part with an empirical spreading of the QP strength and the gross theory for the first-forbidden part of β^- decay. Nuclear masses are either taken from the 1995 data compilation of Audi *et al.*, when available, otherwise from the finite-range droplet model. Especially for spherical and neutron-(sub-)magic isotopes a considerable improvement compared to our earlier predictions for pure GT decay (ADNDT, 1997) is observed. $T_{1/2}$ and P_n values up to the neutron drip line have been used in *r*-process calculations within the classical ''waiting-point'' approximation. With the new nuclear-physics input, a considerable speeding-up of the *r*-matter flow is observed, in particular at those *r*-abundance peaks which are related to magic neutron-shell closures.

DOI: 10.1103/PhysRevC.67.055802 PACS number(s): 23.40.−s, 26.30.+k, 97.60.Bw, 98.80.Ft

I. INTRODUCTION

Interactions between astrophysics and nuclear physics have been long standing and rewarding. To the nuclear physicist many phenomena in the universe represent nuclear experiments on a grand scale, often under conditions that cannot be replicated on earth. To the astrophysicist nuclear physics represents experimental and theoretical sources of data which are needed to model the energy balances and time scales in many astrophysical scenarios. Examples of this dichotomy are the explanation of the source of the energy production in the sun and the postulation of a rapid-neutron-capture process, or *r* process [1–3], as the origin of many heavy nuclei beyond Fe.

To us, modeling the *r* process has represented a particularly fascinating challenge. Its detailed study requires input of nuclear data from experiment and/or theory. However, properly designed studies can also provide information to the nuclear theorist on nuclear properties far from stability that are inaccessible to experimental study. Informative studies of the *r* process can be accomplished with a knowledge of just a few nuclear properties, namely, the nuclear mass (from which neutron separation energies S_n and β-decay Q_β values can trivially be obtained), the β-decay half-lives $T_{1/2}$, and β-delayed neutron-emission probabilities $P_{\nu n}$. More elaborate studies require additional quantities such as reaction rates and temperature dependences of many quantities.

A great leap forward in our understanding of the *r* process and other stellar nucleosynthesis processes took place about 10 years ago, when data from global, unified, microscopic nuclear-structure models for the nuclear mass and β decay were used for the first time in such calculations [4]. A key new feature was the reliability of some nuclear-structure models, based on microscopic Schrödinger equations, also outside the regions where the model parameters were determined. That is, they are reliable also for regions of neutron-rich nuclei beyond the experimentally known region near β stability. Most influential in the first studies of this type were the ''Möller-Nix'' mass models and the ''Krumlinde-Möller-Randrup'' quasiparticle random-phase (QRPA) model of β decay. The first ''Möller-Nix'' mass model was published in 1981 [5]; its current enhanced form [finite-range droplet model (FRDM), 1992] was finalized in 1992 and published in 1995 [6]. The initial QRPA model is from 1984 [7] with numerous enhancements added over the next several years. An extensive discussion of the enhanced model was published in 1990 [8]. Tabulated β-decay properties for 8979 nuclei from ^{16}O and beyond appeared in 1997 [9].

There are only a very few realistic mass models in which microscopic effects are calculated from microscopic effective interactions. Single-particle potentials in the macroscopic-microscopic approach and two-body Skyrme-type potentials in Hartree-Fock models are two examples of such ''microscopic'' interactions. Examples of calculations based on such potentials are, apart from the work mentioned above, the early work by Seeger and Howard [10] in a macroscopic-microscopic approach and more current work based on Skyrme interactions [11–13]. All these mass models have an rms error of about 0.7 MeV in the region where the model constants were adjusted, and do not diverge, so far, outside the region of adjustment. That is, when new masses are measured and compared to published masses the rms error is still about 0.7 MeV. Despite such errors much has been learned about the *r* process from calculations based on these nuclear data sources.

It is noteworthy that for 20 years the error of the realistic, extrapolatable mass models has remained fairly constant at about 0.7 MeV (our 1981 mass model error was 0.835 MeV). Very recently, we have even seen results of the first self-

consistent Hartree-Fock (HF) mass model with two-body Skyrme-type forces with optimized parameters. Also in this approach the mass model rms error is near 0.7 MeV. A recent analysis by Bohigas and Lebœuf [14,15] proposes that this empirically observed lower limit is actually obtained as a lower limit for the error for models of this type from very general and fundamental arguments. Because of correlations in the mass errors for nuclei close to each other in the nuclear chart, this translates to about ± 0.5 MeV errors in calculated Q_β and S_n values. It may therefore be very difficult to develop mass models that are not subject to these limitations. In our efforts to improve the nuclear data input of our astrophysical *r*-process calculations, we therefore in our new studies here focus less on the mass models and the masses they produce, and instead concentrate on the β-decay models from which we obtain decay half-lives. The former data influence the *structure* of the *r* abundances whereas the latter relate directly to the *time scale* of the *r* process. However, due to correlations of Q_β and S_n errors with calculated β-decay properties again for nuclei far from stability $T_{1/2}$ and P_n values can only be predicted within about a factor 2 to 3. We present some basic aspects of the 1990 version of our β-decay model and then introduce and justify two enhancements to this model. Subsequently, we investigate the consequences of the model improvements on *r*-process calculations.

II. MODELS

Theoretically, the two integral β-decay quantities, $T_{1/2}$ and P_n, are interrelated via their usual definition in terms of the so-called β-strength function $[S_\beta(E)]$ [16],

$$1/T_{1/2} = \sum_{0 \leqslant E_i \leqslant Q_\beta} S_\beta(E_i) \times f(Z,R,Q_\beta - E_i), \qquad (1)$$

where R is the nuclear radius, Q_β is the maximum β-decay energy (or the isobaric mass difference), and $f(Z,R,Q_\beta - E_i)$ the Fermi function. With this definition, $T_{1/2}$ may yield information on the *average* β feeding of a nucleus. However, since transition rates to low-lying daughter states are strongly enhanced by the phase-space factor of β decay, $f \sim (Q_\beta - E_i)^5$, the largest contribution to $T_{1/2}$ comes from decays to the lowest-energy resonances in $S_\beta(E_i)$; that is, from the (near-) ground-state allowed Gamow-Teller (GT) or first-forbidden (ff) transitions.

The β-delayed neutron emission probability (P_n) is schematically given by

$$P_n = \frac{\sum_{S_n}^{Q_\beta} S_\beta(E_i) f(Z,R,Q_\beta - E_i)}{\sum_{0}^{Q_\beta} S_\beta(E_i) f(Z,R,Q_\beta - E_i)}, \qquad (2)$$

thus defining P_n as the ratio of the integral β intensity to states above the neutron separation energy S_n to the total β intensity. As is done in nearly all P_n calculations, in the above equation, the ratio of the partial widths for *l*-wave neutron emission $[\Gamma_n^j(E_n)]$ and the total width $[\Gamma_{tot} = \Gamma_n^j(E_n) + \Gamma_\gamma]$ is set equal to 1; i.e., possible γ decay from neutron-unbound levels is neglected. Again, because of the $(Q_\beta - E)^5$ dependence of the Fermi function, the physical significance of the P_n quantity is limited, too. It mainly reflects the β feeding to the energy region just beyond S_n. However, taking together the two gross decay properties, $T_{1/2}$ and P_n, may well provide some first information about the nuclear structure determining β decay. Generally speaking, for a given Q_β value a *short* half-life usually correlates with a *small* P_n value, and vice versa. This is actually more than a simple rule of thumb; it can be used to check the consistency of experimental numbers. Sometimes even global plots of double ratios of experimental to theoretical P_n to $T_{1/2}$ relations are used to show systematic trends, see, for example, Ref. [17]. Several impressive examples in the literature show that it is sometimes possible to identify special nuclear-structure features solely from $T_{1/2}$ and P_n. Among them are: (i) the development of single-particle (SP) structures and related ground-state shape changes in the $50 \leqslant N \leqslant 60$ region of the Sr isotopes [7,18]; (ii) the prediction of the at that time totally unexpected collectivity of the neutron-magic nucleus ($N=28$) ^{44}S situated two proton pairs below the doubly magic ^{48}Ca [19]; and (iii) the very recent interpretation of the surprising decay properties of ^{131,132}Cd just above $N=82$ [20–22].

Today, in studies of nuclear-structure features, even of gross properties such as the $T_{1/2}$ and P_n values considered here, a substantial number of different theoretical approaches are used. The significance and sophistication of these models and their relation to each other should, however, be clear before they are applied. In general, one can assign the nuclear models used to calculate the above two decay properties to the following different groups.

(1) *Models where the physical quantity of interest is given by a polynomial or some other algebraic expression*. Normally, the parameters are determined by adjustments to experimental data and the models only describe a single nuclear property. No nuclear wave functions are obtained in these models. Examples of theories of this type are purely empirical approaches that assume a specific shape of $S_\beta(E)$ (either constant or proportional to level density), such as the Kratz-Herrmann formula [23] or the statistical gross theory of β decay [24,25]. These models can be considered to be analogous to the liquid-drop model of nuclear masses, and are—again—appropriate for dealing with *average* properties of β decay. In these approaches, it is inherent that no insight into the underlying SP structure is possible.

(2) *Models that use an effective nuclear interaction and usually solve the microscopic quantum-mechanical Schrödinger or Dirac equation*. The approaches that actually do solve the Schrödinger equation provide nuclear wave functions that allow a variety of nuclear properties (e.g., ground-state shapes, level energies, spins and parities, transition rates, $T_{1/2}$, $P_{\nu n}$, etc.) to be modeled within a single framework. Most theories of this type that are currently used in large-scale calculations, such as the FRDM+QRPA model [9] used here or the ETFSI+cQRPA approach [11,26], in

principle fall into two subgroups, depending on the type of microscopic interaction used. Another aspect of these models is whether they are restricted to spherical shapes, to even-even isotopes, or whether they can describe all nuclear shapes and all types of nuclei. Examples of this type of models are the following.

(a) SP approaches that use a simple central potential with additional residual interactions. The Schrödinger equation is solved in the SP potential and additional two-body interactions may be treated in the BCS, Lipkin-Nogami, or random-phase approximation. The nuclear potential energy as a function of shape is calculated by combining the SP model with a macroscopic model in the so-called macroscopic-microscopic method. Within this approach, the nuclear ground-state energy is calculated as a sum of a microscopic correction obtained from the SP levels by use of the Strutinsky method and a macroscopic energy.

(b) Hartree-Fock-type models, in which the postulated effective interaction is of a two-body type. If the microscopic Schrödinger equation is solved then the wave functions obtained are antisymmetrized Slater determinants. In such models, it is possible to obtain the nuclear ground-state energy as $E=\langle\Psi_0|H|\Psi_0\rangle$, otherwise the HF models have many similarities to those in category 2(a) but have fewer parameters.

In principle, models in group 2(b) are expected to be more accurate, because the wave functions and effective interactions can, in principle, be more realistic. However, two problems still remain today: what effective interaction is sufficiently realistic to yield more accurate results, and what are the optimized parameter values for such a two-body interaction?

Some models in category 2 have been overparametrized, which means that their microscopic origins have been lost and the results are just parametrizations of the experimental data. An example of such models is found in Ref. [27], where the strength of the residual GT interaction has been fitted for each element (Z number) in order to obtain optimum reproduction of known $T_{1/2}$ and P_{n} values in each isotopic chain.

To conclude this section, let us emphasize that there is no ''correct'' model in nuclear physics. Any modeling of nuclear-structure properties involves approximations of the true forces and equations with the goal to obtain a formulation that can be solved in practice, but that ''retains the essential features'' of the true system under study, so that one can still learn something. What we mean by this, depends on the actual circumstances. It may well turn out that when proceeding from a simplistic, macroscopic approach to a more microscopic model, the first overall result may be ''worse'' just in terms of agreement between calculated and measured data. However, the disagreements may now be understood more easily, and further microscopic-based, realistic improvements will become possible.

III. PREDICTION OF $T_{1/2}$ AND P_{n} VALUES FROM FRDM-QRPA

A. Model

The formalism we use to calculate GT β-strength functions is fairly lengthy since it involves adding pairing and Gamow-Teller residual interactions to the folded-Yukawa single-particle Hamiltonian and solving the resulting Schrödinger equation in the QRPA. Because this model has been completely described in two previous papers [7,8] we refer to those two publications for a full model specification and for a definition of notation used. We restrict the discussion here to an overview of features that are particularly relevant to the results discussed in this paper.

It is well known that wave functions and transition matrix elements are more affected by small perturbations to the Hamiltonian than are the eigenvalues. When transition rates are calculated it is therefore necessary to add residual interactions to the folded-Yukawa single-particle Hamiltonian, in addition to the pairing interaction that is included in the mass model. Fortunately, the residual interaction may be restricted to a term specific to the particular type of decay considered. To obtain reasonably accurate half-lives it is also very important to include ground-state deformations. Originally, the QRPA formalism was developed for and applied only to spherical nuclei [28–30]. The extension to deformed nuclei, which is necessary in global calculations of β-decay properties, was first described in 1984 [7]. The Gamow-Teller force in our model is given by

$$V_{\mathrm{GT}}=2\chi_{\mathrm{GT}}:\boldsymbol{\beta}^{1-}\cdot\boldsymbol{\beta}^{1+}, \tag{3}$$

which is added to the folded-Yukawa single-particle Hamiltonian after pairing has already been incorporated, with the standard choice $\chi_{\mathrm{GT}}=23$ MeV/A [7,8,28,29].

Here $\boldsymbol{\beta}^{1\pm}=\Sigma_i\boldsymbol{\sigma}^{\pm}_{it_i}$ are the Gamow-Teller $\beta^{\pm}$-transition operators and the colon notation signifies that all contractions in the quasiparticle expansion are ignored.

The process of β decay occurs from an initial ground state or excited state in a mother nucleus to a final state in the daughter nucleus. For β^- decay, the final configuration is a nucleus in some excited state or its ground state, an electron (with energy E_{e}), and an antineutrino (with energy E_ν). The decay rate w_{fi} to one nuclear state f is

$$w_{fi}=\frac{m_0c^2}{\hbar}\frac{\Gamma^2}{2\pi^3}|M_{fi}|^2 f(Z,R,\epsilon_0), \tag{4}$$

where R is the nuclear radius and $\epsilon_0=E_0/m_0c^2$, with m_0 the electron mass and E_0 the energy release in the decay. Moreover, $|M_{fi}|^2$ is the nuclear matrix element, which is also the β-strength function, apart from a constant B defined below:

$$S_\beta(E_i)=|M_{fi}|^2\times\frac{1}{B}. \tag{5}$$

The dimensionless constant Γ is defined by

$$\Gamma\equiv\frac{g}{m_0c^2}\left(\frac{m_0c}{\hbar}\right)^3, \tag{6}$$

where g is the Gamow-Teller coupling constant. The quantity $f(Z,R,\epsilon_0)$ has been extensively discussed and tabulated elsewhere [31–33].

For the special case in which the two-neutron separation energy S_{2n} in the daughter nucleus is greater than Q_β, the energy released in ground-state to ground-state β decay, the probability for β-delayed one-neutron emission, in percent, is given by

$$P_{1n}=100\frac{\sum_{S_{1n}<E_f<Q_\beta} w_{fi}}{\sum_{0<E_f<Q_\beta} w_{fi}}, \tag{7}$$

where $E_f=Q_\beta-E_0$ is the excitation energy in the daughter nucleus and S_{1n} is the one-neutron separation energy in the daughter nucleus. We assume that decays to energies above S_{1n} always lead to delayed neutron emission.

To obtain the half-life with respect to β decay, one sums up the decay rates w_{fi} to the individual nuclear states in the allowed energy window. The half-life is then related to the total decay rate by

$$T_\beta=\frac{\ln 2}{\sum_{0<E_f<Q_\beta} w_{fi}}. \tag{8}$$

The above equation may be rewritten as

$$T_\beta=\frac{\hbar}{m_0c^2}\frac{2\pi^3\ln 2}{\Gamma^2}\frac{1}{\sum_{0<E_f<Q_\beta}|M_{fi}|^2 f(Z,R,\epsilon_0)}$$

$$=\frac{B}{\sum_{0<E_f<Q_\beta}|M_{fi}|^2 f(Z,R,\epsilon_0)}, \tag{9}$$

with

$$B=\frac{\hbar}{m_0c^2}\frac{2\pi^3\ln 2}{\Gamma^2}. \tag{10}$$

For the value of B corresponding to Gamow-Teller decay we use [7,8]

$$B=4131\ \text{s}. \tag{11}$$

The energy released in ground-state to ground-state electron decay is given in terms of the atomic mass excess $M(Z,N)$ or the total binding energy $E_{\text{bind}}(Z,N)$ by

$$Q_{\beta^-}=M(Z,N)-M(Z+1,N-1). \tag{12}$$

The above formulas apply to the β^- decays that are of interest here. The decay Q values and neutron separation energies $S_{\nu n}$ are obtained from our FRDM mass model when experimental data are unavailable [6,9]. The matrix elements M_{fi} are obtained from our QRPA model. More details are provided elsewhere [8].

B. Calculated results

We compare here two calculations. The first is our original model as described in Ref. [8] with the following enhancements.

To calculate β-decay Q values and neutron separation energies $S_{\nu n}$ we use experimental ground-state masses where available, otherwise calculated masses [6]. In our previous recent calculations we used the 1989 mass evaluation [34]; here we use the 1995 mass evaluation [35].

It is known that at higher excitation energies additional residual interactions result in a spreading of the transition strength. In our 1997 calculation each transition goes to a precise, well-specified energy in the daughter nucleus. This can result in very large changes in the calculated P_n values for minute changes in, for example, S_{1n}, depending on whether an intense, sharp transition is located just below or just above the neutron separation energy [8]. To remove this unphysical feature we introduce an empirical spreading width that sets in above 2 MeV. Specifically, each transition strength ''spike'' above 2 MeV is transformed to a Gaussian of width

$$\Delta_{\text{sw}}=\frac{8.62}{A^{0.57}}. \tag{13}$$

This choice is equal to the error in the mass model. Thus, it accounts approximately for the uncertainty in calculated neutron separation energies and at the same time it roughly corresponds to the observed spreading of transition strengths in the energy range 2–10 MeV, which is the range of interest here [36–40]. The results are insensitive to the exact choice of spreading width.

We also base our calculations on more correct ground-state deformations that affect the energy levels and wave functions that are obtained in the single-particle model. The ground-state deformations calculated in the FRDM mass model (Möller *et al.*, 1992), generally agree with experimental observations, but in transition regions between spherical and deformed nuclei discrepancies do occur. We therefore replace calculated deformations with spherical shape, when experimental trends so indicate. This has been done for the following nuclides: $^{67-78}$Fe, $^{67-79}$Co, $^{73-80}$Ni, $^{73-81}$Cu, $^{78-84}$Zn, $^{79-87}$Ga, $^{83-90}$Ge, $^{84-91}$As, $^{87-94}$Se, $^{87-96}$Br, $^{92-98}$Kr, $^{91-96}$Rb, ^{96,97}Sr, $^{96-98}$Y, $^{134-140}$Sb, $^{136-141}$Te, $^{137-142}$I, $^{141-143}$Xe, and $^{141-145}$Cs. In the second calculation we account for the effect of ff strength, calculated in the statistical gross theory [24,25], on the decay half-lives and β-delayed neutron-emission probabilities. Relative to the allowed Gamow-Teller strength, which over a given energy range is represented by relatively few strong peaks, the ff strength with its numerous small, densely spaced, peaks to a good approximation constitutes a ''smooth background.'' It is therefore a reasonable approach to calculate the GT tran-

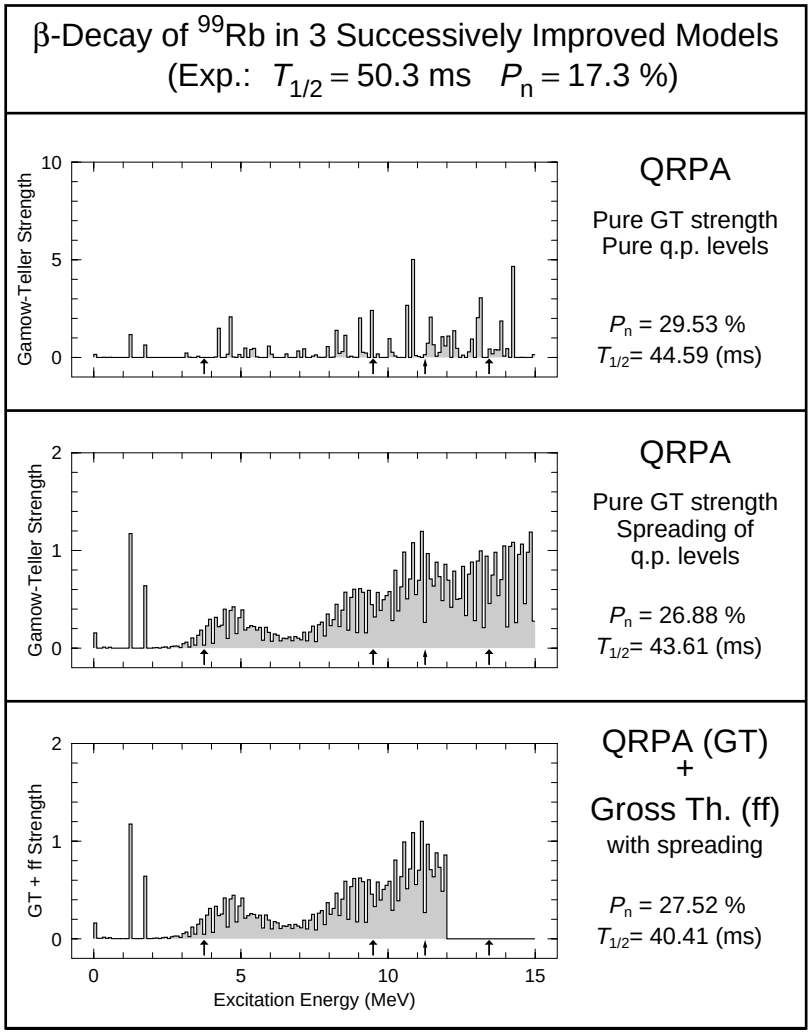

FIG. 1. Calculated β-strength functions, corresponding half-lives, and delayed-neutron emission probabilities for ^{99}Rb in three successively enhanced models. The narrow arrow indicates the Q_β value, the wide arrows successive neutron-separation energies; the lowest arrow S_{1n}, the second lowest S_{2n}, and so on. The results are further discussed in the text.

sitions in a microscopic QRPA approach and the ff transitions in a macroscopic statistical model, in analogy with the macroscopic-microscopic method in which the nuclear energy as a function of shape is calculated as a sum of a liquid-drop-type model that varies smoothly with proton number, neutron number, and deformation and a shell-correction part that exhibits rapid variation in these variables. Strictly speaking, $f(Z,R,\epsilon_0)$ is different for allowed and first-forbidden transitions. Here we use the same $f(Z,R,\epsilon_0)$ in both cases, a negligible approximation in our statistical model of the first-forbidden decays.

We show in Figs. 1–3 three representative examples of the effect of two of our model enhancements on the strength functions, half-lives, and delayed neutron probabilities for ^{99}Rb, ^{92}Rb, and ^{137}I. The top subplot shows the original model, the middle subplot the effect of spreading the transition strength, and the bottom subplot the effect of also including ff transitions.

The first case, ^{99}Rb in Fig. 1, is a well-deformed nucleus. In the original model there is significant strength at low energies, as is often the case in deformed nuclei. Therefore there is for this nucleus little effect of our two model enhancements: strength spreading and inclusion of ff transitions. In contrast, for the spherical ^{92}Rb nucleus shown in Fig. 2 and for ^{137}I in Fig. 3 the effect of the two improvements is dramatic. We have chosen ^{92}Rb as one illustrative example for two reasons. First, in the standard model calculation, illustrated in the top subplot, S_{1n} sits just below the first major peak in the strength function, with some strength, not discernable on this plot occurring below the one-neutron separation energy. This leads to a very high delayed-neutron emission probability, in contradiction to experiment. Second, most of the strength occurring within the Q_β window lies *just below* Q_β. Therefore we obtain a half-life of the order of hours, again in contradiction with experiment. Already after implementing the first model enhancement, the spreading of the GT strength, the agreement with experiment improves considerably: the half-life is reduced by a factor of 6.5 and the delayed-neutron emission probability by a factor of 20. In the next step there are even more dramatic changes in the calculated half-life and neutron-emission probability and the agreement with experiment is now quite good. The last case, ^{137}I, has been chosen as a typical example of nuclei in the heavy fission-peak mass region where—consistently—there is no low-lying GT strength. In the initial model there are large differences between the calculated and experimental $T_{1/2}$ and P_n values. The effect of the spreading of the GT

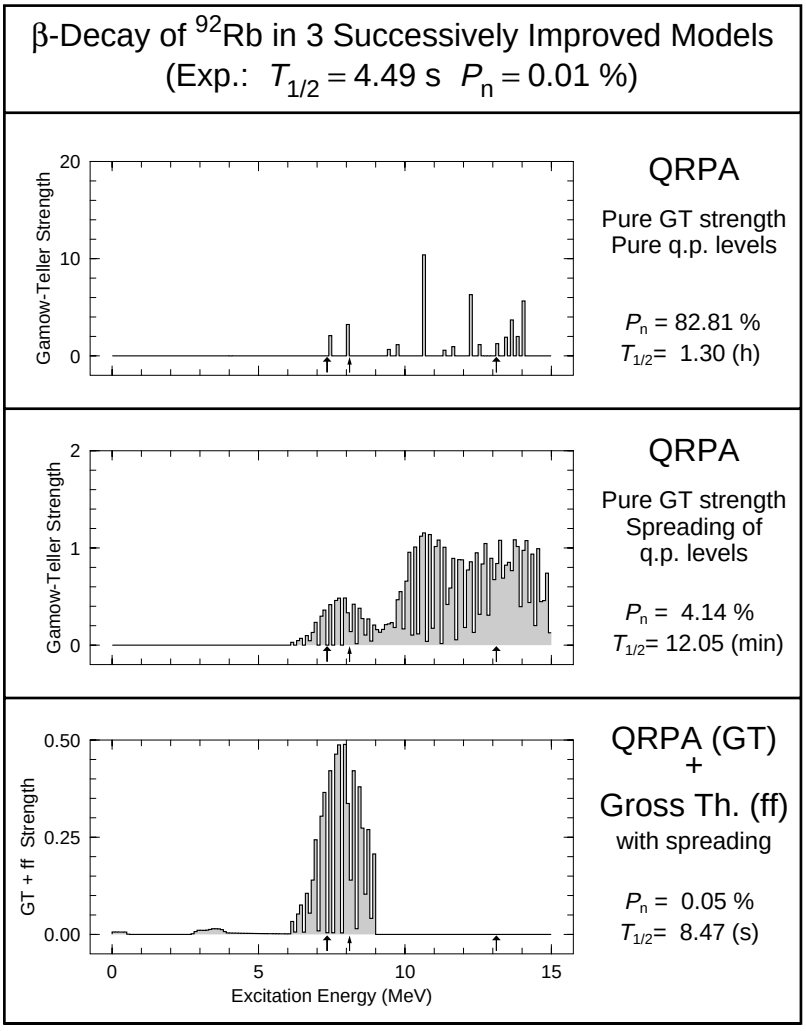

FIG. 2. Calculated β-strength functions, corresponding half-lives, and delayed-neutron emission probabilities for ^{92}Rb in three successively enhanced models. The narrow arrow indicates the Q_β value, the wide arrows successive neutron-separation energies; the lowest arrow S_{1n}, the second lowest S_{2n}, and so on. The results are further discussed in the text.

strength is somewhat less dramatic than for ^{92}Rb but after the ff strength is included we again achieve good agreement with experimental data.

It is not our aim here to make a detailed analysis of each individual nucleus, but instead to present an overview of the model performance in a calculation of a large number of β-decay half-lives and delayed neutron-emission probabilities. In Figs. 4 and 5 we compare measured β^--decay half-lives and β-delayed neutron-emission probabilities with calculations based on our two models, for nuclei throughout the periodic system. To address the reliability versus distance from stability, we present the ratio $T_{\beta,\mathrm{calc}}/T_{\beta,\mathrm{exp}}$ versus the quantity $T_{\beta,\mathrm{exp}}$. Because the relative error in the calculated half-lives is more sensitive to small shifts in the positions of the calculated single-particle levels for decays with small energy releases, where long half-lives are expected, one can anticipate that half-life calculations are more reliable far from stability, where the β-decay Q values are large, than close to β-stable nuclei (see Table I).

Furthermore, because the Fermi function is dominated by the phase space factor $(Q_\beta - E_f)^5$, where E_f is the excitation energy of the final state in the daughter nucleus, it is clear that the same absolute error ΔE in the calculated Q_β value will result in a smaller error in $T_{1/2}$ for large Q_β than for small Q_β. Since Q_β increases quite rapidly with distance from β stability (for example, for ^{94}Sr Q_β is 2.36 MeV and for ^{100}Sr it is 6.86 MeV) we expect for this reason alone that the errors in the calculated half-lives will decrease with increasing distance from stability even if Q_β were to develop somewhat increasing errors.

Before we make a quantitative analysis of the agreement between calculated and experimental half-lives we briefly discuss what conclusions can be drawn from a simple visual inspection of Fig. 4. As a function of $T_{\beta,\mathrm{exp}}$ one would expect the average error to increase as $T_{\beta,\mathrm{exp}}$ increases. This is indeed the case in both of the model calculations. When, as in the lower part of the figure, ff transitions are included the agreement between calculations and experiment is better, in particular for long half-lives, as expected, because for the small decay Q values here the ff transitions are relatively more important. In addition, one is left with the impression that the errors in our calculation are fairly large. However, this is partly a fallacy, since for small errors there are many more points than for large errors. This is not clearly seen in the figures, since for small errors many points are superimposed on one another. To obtain a more exact understanding of the error in the calculation we therefore perform a more detailed analysis.

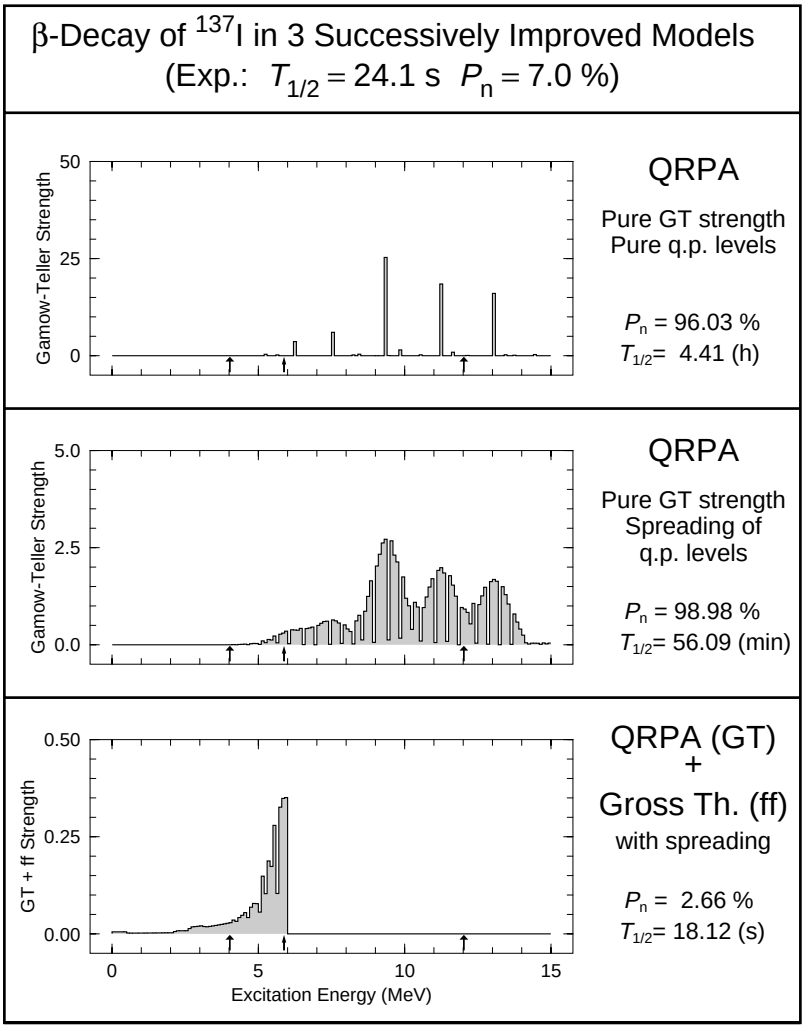

FIG. 3. Calculated β-strength functions, corresponding half-lives, and delayed-neutron emission probabilities for ^{137}I in three successively enhanced models. The narrow arrow indicates the Q_β value, the wide arrows successive neutron-separation energies; the lowest arrow S_{1n}, the second lowest S_{2n}, and so on. The results are further discussed in the text.

C. Error analysis

One often analyzes the error in a calculation by studying a root-mean-square (rms) deviation, which in this case would be

$$\sigma_{\mathrm{rms}}{}^2=\frac{1}{n}\sum_{i=1}^{n}(T_{\beta,\mathrm{exp}}-T_{\beta,\mathrm{calc}})^2. \tag{14}$$

However, such an error analysis is unsuitable here, for two reasons. First, the quantities studied vary by many orders of magnitude. Second, the calculated and measured quantities may *differ* by orders of magnitude. We therefore study the quantity $\log_{10}(T_{\beta,\mathrm{calc}}/T_{\beta,\mathrm{exp}})$, which is plotted in Fig. 4, instead of $(T_{\beta,\mathrm{exp}}-T_{\beta,\mathrm{calc}})^2$. We present the formalism here for the half-life, but the formalism is also used to study the error of our calculated P_n values.

To facilitate the interpretation of the error plots we consider two hypothetical cases. As the first example, suppose that all the points were grouped on the line $T_{\beta,\mathrm{calc}}/T_{\beta,\mathrm{exp}}=10$. It is immediately clear that an error of this type could be entirely removed by introducing a renormalization factor, which is a common practice in the calculation of β-decay half-lives. We shall see below that in our model the half-lives corresponding to our calculated strength functions have about zero average deviation from the calculated half-lives, so no renormalization factor is necessary.

In another extreme, suppose half the points were located on the line $T_{\beta,\mathrm{calc}}/T_{\beta,\mathrm{exp}}=10$ and the other half on the line $T_{\beta,\mathrm{calc}}/T_{\beta,\mathrm{exp}}=0.1$. In this case the average of $\log_{10}(T_{\beta,\mathrm{calc}}/T_{\beta,\mathrm{exp}})$ would be zero. We are therefore led to the conclusion that there are several types of errors that are of interest to study; namely, the average position of the points in Fig. 4, which is just the average of the quantity $\log_{10}(T_{\beta,\mathrm{calc}}/T_{\beta,\mathrm{exp}})$, and the spread of the points around this average. To analyze the error along these ideas, we introduce the quantities

$$r=T_{\beta,\mathrm{calc}}/T_{\beta,\mathrm{exp}}, \tag{15}$$

$$r_1=\log_{10}(r),$$

$$M_{r_1}=\frac{1}{n}\sum_{i=1}^{n} r_1^i,$$

$$M_{r_1}^{10}=10^{M_{r_1}} \quad [\text{mean deviation (factor)}],$$

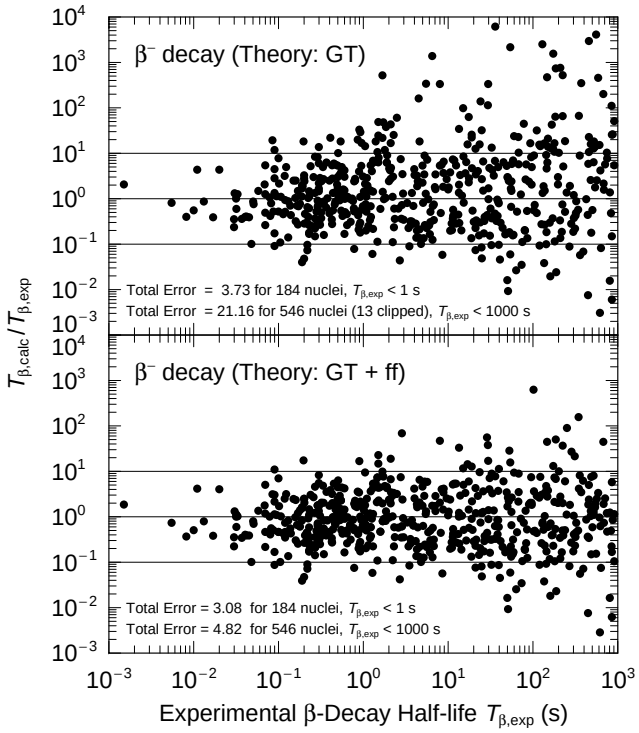

FIG. 4. Ratio of calculated to experimental β^--decay half-lives for nuclei from ^{16}O to the heaviest known in our previous and current models. The β-decay rates of *r*-process nuclei are normally shorter than 150 ms.

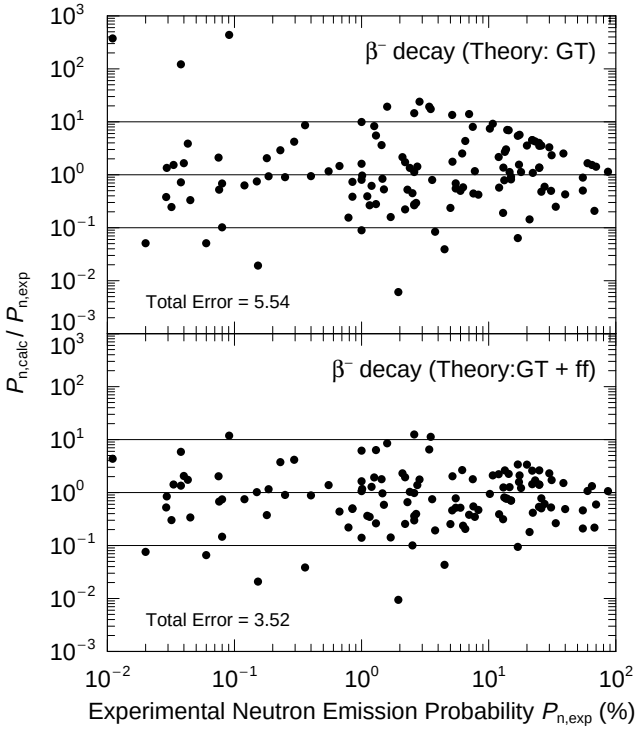

FIG. 5. Ratio of calculated to experimental β-delayed neutron-emission probabilities P_n for nuclei in the fission-fragment region in our previous and current models.

$$\sigma_{r_1}=\left[\frac{1}{n}\sum_{i=1}^{n}(r_1^i-M_{r_1})^2\right]^{1/2},$$

$$\sigma_{r_1}^{10}=10^{\sigma_{r_1}} \quad [\text{mean fluctuation (factor)}],$$

$$\Sigma_{r_1}=\left[\frac{1}{n}\sum_{i=1}^{n}(r_1^i)^2\right]^{1/2}, \quad \text{and}$$

$$\Sigma_{r_1}^{10}=10^{\Sigma_{r_1}} \quad [\text{total error (factor)}],$$

where M_{r_1} is the average position of the points and σ_{r_1} is the spread around this average. When we prefer to represent the error by a single number we use the measure $\Sigma_{r_1}^{10}$ for the ''total'' error factor. The spread σ_{r_1} can be expected to be related to uncertainties in the positions of the levels in the underlying single-particle model. The use of a logarithm in the definition of r_1 implies that these two quantities correspond directly to distances as seen by the eye in, for example, Fig. 4, in units where one order of magnitude is 1. After the error analysis has been carried out we want to discuss its result in terms like ''on the average the calculated half-lives are 'a factor of 2' too long.'' To be able to do this we must convert back from the logarithmic scale. Thus, we realize that the quantities $M_{r_1}^{10}$ and $\sigma_{r_1}^{10}$ are conversions back to ''factor of'' units of the quantities M_{r_1} and σ_{r_1}, which are expressed in distance or logarithmic units.

We are now in a position to analyze the deviations between our calculations and experiment. An analysis of the half-life comparisons in Fig. 4 is given in Table I and of the β-delayed neutron-emission probability comparisons in Fig. 5 in Table II. The half-life comparison shows, as earlier [8,9], that the mean deviation of the calculated half-lives from the experimental values is approximately zero, that is, $M_{r_1}\approx 0$. Thus, no ''renormalization'' of the calculated β strength is indicated. This is true both for the GT calculation, and in particular for the GT+ff calculation. A large mean error is obtained for the GT calculation when nuclei with very long half-lives are included. This does not indicate a need for a general renormalization, because the calculated half-lives of nuclei with short half-lives are correct on the average. Rather, the deviations of the mean half-lives occur because the effect of ff strength is not considered in GT-only calculation. When the ff strength is included, the mean deviation is always very close to zero. In addition, in the GT + ff case the total error factor $\Sigma_{r_1}^{10}$ increases only very slowly when nuclei with very long half-lives are included in the calculations. This increase is expected because when the Q_β window becomes increasingly small the calculated half-life values are more sensitive to small errors in the calculated positions in energy of the GT transitions.

For delayed-neutron emission there are fewer data points available than for β-decay half-lives. However, the more than 100 data points [41] are sufficient to allow us to draw several conclusions. First, just as for the half-lives we find that the calculations are more accurate for decays corresponding to large Q_β values; that is, far from stability, where

TABLE I. Analysis of the discrepancy between calculated and measured β^--decay half-lives shown in Fig. 4. Each line uses an experimental dataset that is limited to nuclei with half-lives shorter than the value given in the last column.

Model	n	M_{r_1}	$M_{r_1}^{10}$	σ_{r_1}	$\sigma_{r_1}^{10}$	Σ_{r_1}	$\Sigma_{r_1}^{10}$	$T_{\beta,\mathrm{exp}}^{\mathrm{max}}$ (s)
GT	546	0.34	2.20	1.28	19.09	1.33	21.17	1000.0
GT+ff	546	−0.04	0.92	0.68	4.81	0.68	4.82	1000.0
GT	431	0.19	1.55	0.94	8.81	0.96	9.21	100.0
GT+ff	431	−0.04	0.91	0.61	4.10	0.61	4.12	100.0
GT	306	0.14	1.38	0.77	5.87	0.78	6.04	10.0
GT+ff	306	−0.03	0.93	0.55	3.52	0.55	3.53	10.0
GT	184	0.03	1.06	0.57	3.72	0.57	3.73	1.0
GT+ff	184	−0.08	0.84	0.48	3.04	0.49	3.08	1.0
GT	137	−0.01	0.97	0.55	3.53	0.55	3.53	0.5
GT+ff	137	−0.09	0.81	0.49	3.10	0.50	3.17	0.5
GT	72	−0.04	0.92	0.54	3.44	0.54	3.45	0.2
GT+ff	72	−0.10	0.80	0.50	3.19	0.51	3.25	0.2
GT	42	−0.03	0.94	0.51	3.24	0.51	3.25	0.1
GT+ff	42	−0.08	0.83	0.47	2.92	0.47	2.97	0.1

data are often not available. Large Q_β values usually correspond to large P_n values. Second, we find also here that including ff transitions in the simple statistical gross theory model considerably improves the calculations.

To gain further insight into the consequences of including ff transitions in our β-strength functions we make several comparisons. In Figs. 6 and 7 we plot $\log_{10}(T_{\mathrm{calc}}/T_{\mathrm{exp}})$ for calculations without and with ff strength included in ''nuclear chart'' form. The results without ff transitions in Fig. 6 are very clear: close to stability, and close to magic numbers, the calculated half-lives are systematically much too long. The calculated half-lives are large near magic numbers also far from stability. This is very undesirable; the consequence will be that the calculated time for the r process to reach the heavy region and to reach a steady-state situation can be expected to be too long compared to the actual duration. The reason for these deviations near β stability and near magic numbers was elaborated in our discussion of Figs. 2 and 3. Figure 7 shows that when ff transitions are included then these systematic deviations largely disappear. The behavior of calculated P_n values, shown in Figs. 8 and 9, is similar. We have substantially fewer data points here, but it is clear that some systematic deviations near β stability disappear when ff transitions are included. In Fig. 10 we plot the ratio of the half-lives calculated without and with ff transitions included. Then neutron separation energies $S_\mathrm{n}=3.0$ and $S_\mathrm{n}=1.5$ are shown as black lines. Nuclear properties in this region are expected to affect the final r abundances. As could be partly concluded already from our discussion of Figs. 6 and 7, we find big differences near β stability and near magic numbers, in this latter case also far from stability. The differences are particularly noticeable just beyond $N=50$ and $N=82$ for nuclei in the vicinity of the r-process line. Above we made the case that the enhanced model with the ff transitions included is the more realistic one.

The calculated half-lives and β-delayed neutron-emission probabilities on which the calculations here are based are available through a Los Alamos National Laboratory web location [42] on the T16 site.

TABLE II. Analysis of the discrepancy between calculated and measured β-delayed neutron-emission probability P_n values shown in Fig. 5. Each line uses an experimental dataset that is limited to nuclei with half-lives shorter than the value given in the last column.

Model	n	M_{r_1}	$M_{r_1}^{10}$	σ_{r_1}	$\sigma_{r_1}^{10}$	Σ_{r_1}	$\Sigma_{r_1}^{10}$	$T_{\beta,\mathrm{exp}}^{\mathrm{max}}$ (s)
GT	126	0.08	1.21	0.74	5.48	0.74	5.54	100.0
GT+ff	126	−0.11	0.78	0.54	3.44	0.55	3.52	100.0
GT	74	0.04	1.10	0.75	5.66	0.74	5.50	10.0
GT+ff	81	−0.14	0.72	0.56	3.67	0.61	4.06	10.0
GT	43	0.06	1.16	0.75	5.66	0.71	5.18	1.0
GT+ff	43	−0.14	0.73	0.65	4.45	0.71	5.17	1.0
GT	16	0.18	1.52	1.08	11.94	0.94	8.80	0.1
GT+ff	19	−0.07	0.86	0.81	6.51	0.85	7.05	0.1

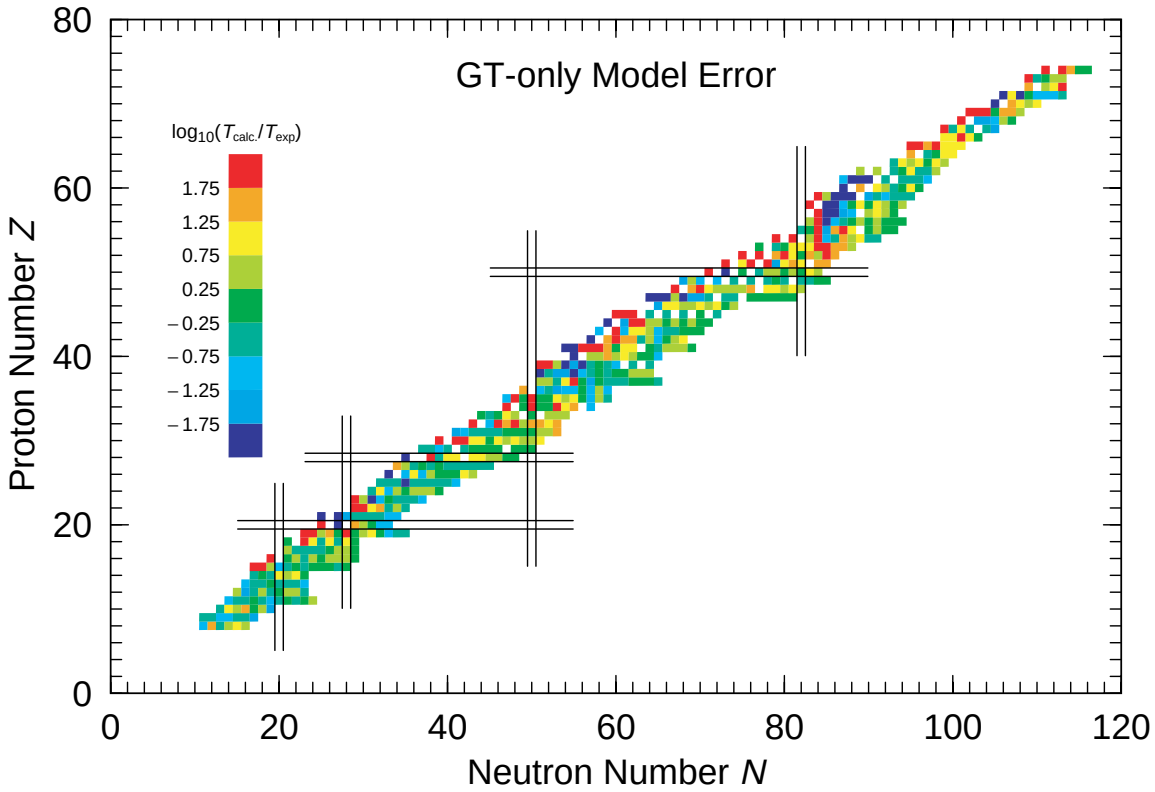

FIG. 6. (Color) Plot of the ratio of calculated to experimental β^--decay half-lives for nuclei from ^{16}O to the heaviest known.

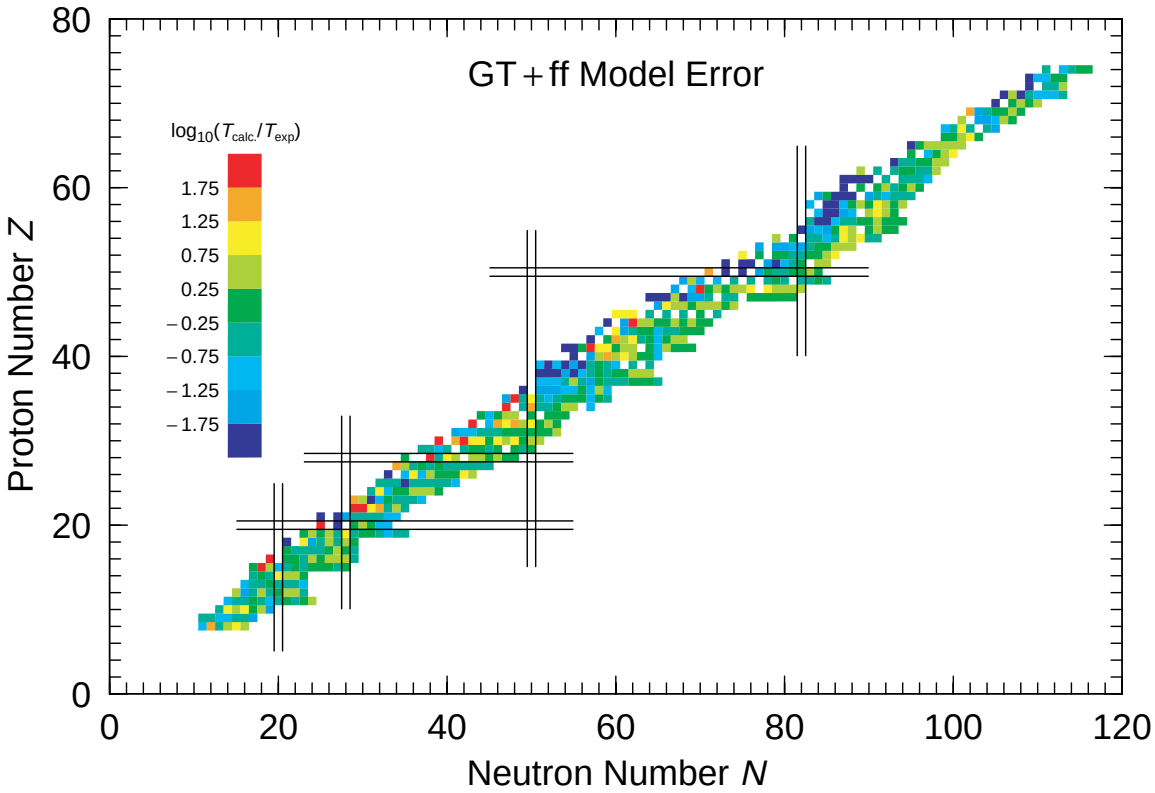

FIG. 7. (Color) Plot of the ratio of calculated to experimental β^--decay half-lives for nuclei from ^{16}O to the heaviest known. In this case first-forbidden transitions, as given by the statistical gross theory, are taken into account.

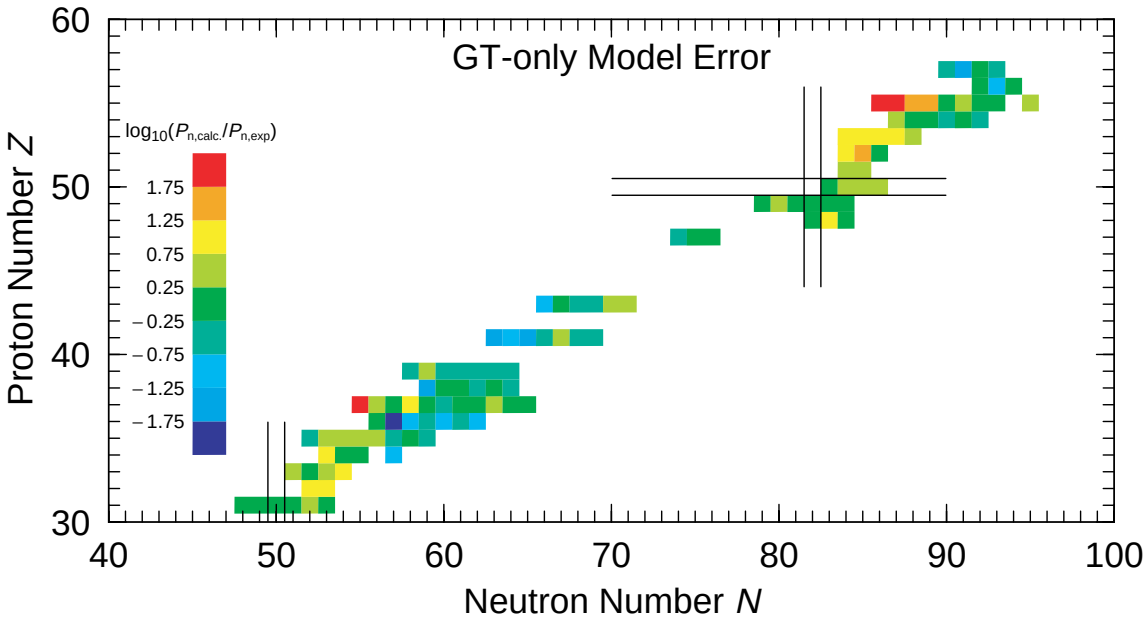

FIG. 8. (Color) Plot of the ratio of calculated to experimental β^--delayed neutron-emission probabilities for nuclei in the fission-fragment region.

IV. SPEEDING-UP THE *r* PROCESS

In order to study the effect of the new theoretical β-decay properties on *r*-process calculations to reproduce the solar-system isotopic *r*-abundance pattern ($N_{r,\odot}$), we use an extension of the classical ''waiting-point'' model which is outlined in detail in Refs. [4,43]. In our present time-dependent calculations we use a superposition of 16 *r*-components with constant neutron densities in the range $10^{20} \leqslant n_n(\mathrm{cm}^{-3}) \leqslant 3 \times 10^{27}$ and a constant (freeze-out) temperature $T_9 = 1.35$ (where T_9 is in units of 10^9 K) over varying process duration times τ_r. This provides a sufficiently narrow n_n grid to obtain convergence in the calculated final isotopic *r* abundances (see, e.g., Ref. [44]). An instantaneous freeze-out of the initial *r*-progenitor distribution was assumed; i.e., neutron captures during decay back to stability were neglected. However, β-delayed emission of one to three neutrons has fully been taken into account using our recent compilation of experimental P_n values [41,45] together with theoretical predictions from either Ref. [9] [P_n(GT)] or the present work [P_n(GT+ff)].

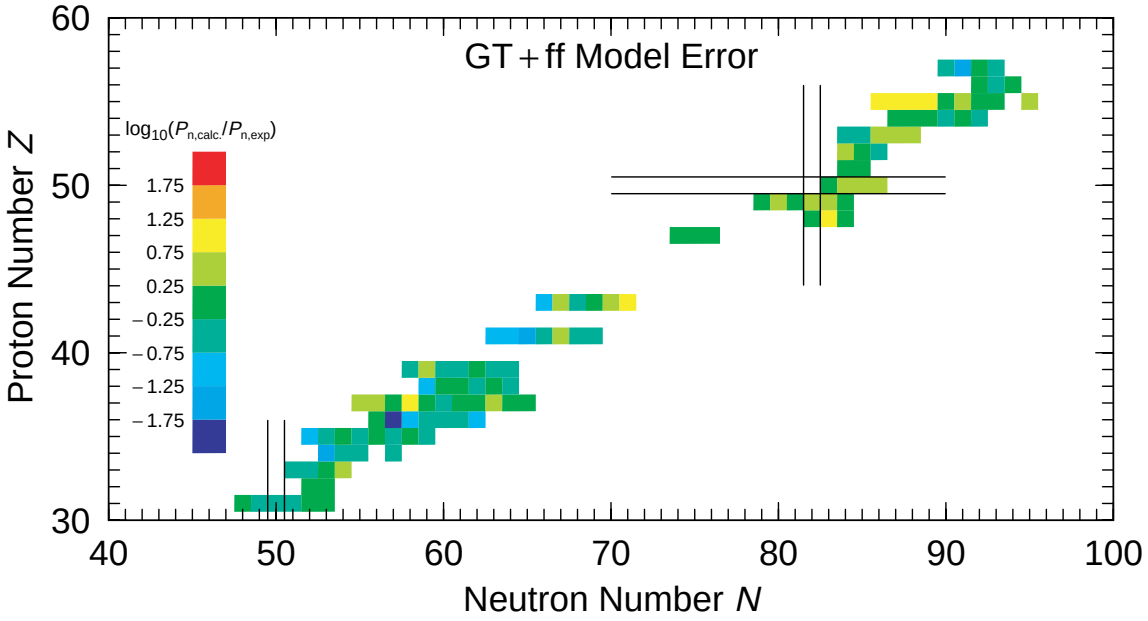

FIG. 9. (Color) Plot of the ratio of calculated to experimental β^--delayed neutron-emission probabilities for nuclei in the fission-fragment region. In this case first-forbidden transitions, as given by the statistical gross theory, are taken into account.

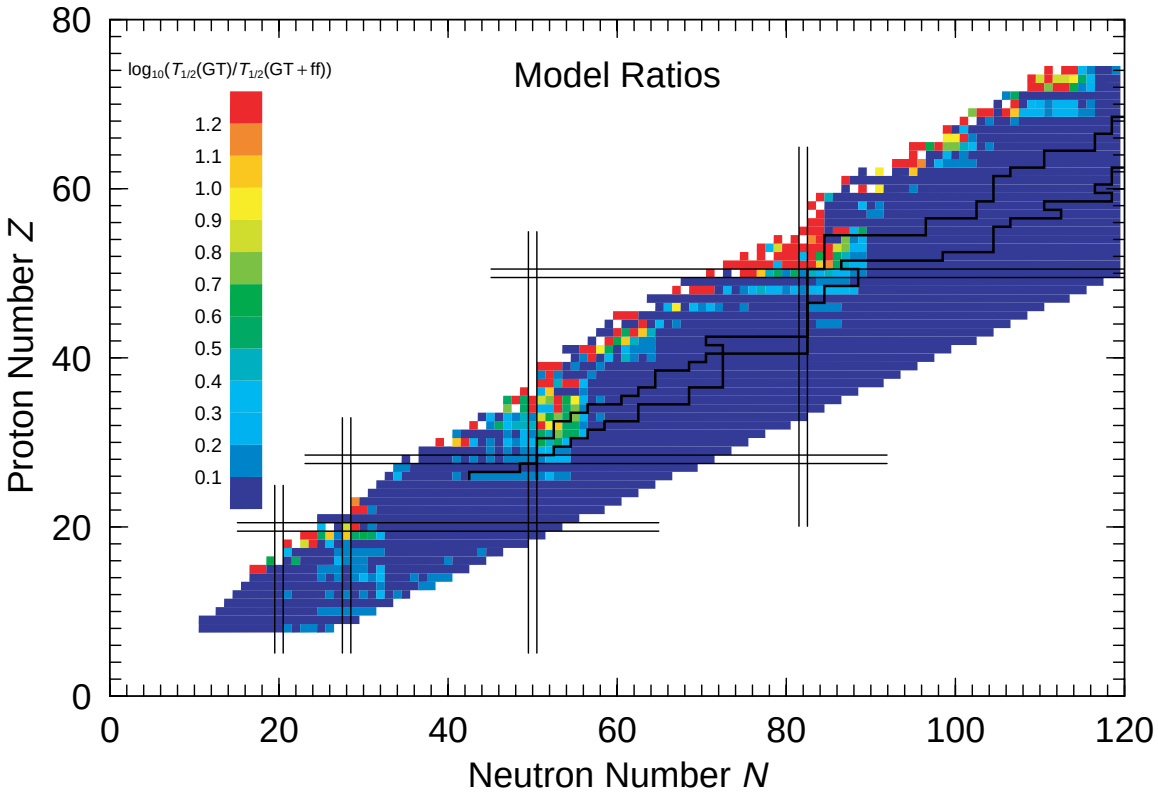

FIG. 10. (Color) Plot of the ratio of calculated β^--decay half-lives without and with first-forbidden transitions included. Then neutron separation energies $S_n=3.0$ and $S_n=1.5$ are shown as black lines. Just beyond $N=50$ and $N=82$ there is a significant decrease of the calculated half-lives in the *r*-process path between these two lines when ff transitions are included.

Since occasionally questions arise concerning our interpretation of how in a simplified *r*-process model the observed *r*-abundance features and nuclear-physics properties far from stability are related, we summarize our main arguments once again. Initially, based on the identification of the first two classical neutron-magic waiting-point isotopes ^{80}Zn and ^{130}Cd [46–48] we have determined the n_n-T_9 conditions of an *r* process required to form the $A\simeq 80$ and $130 N_{r,\odot}$ peaks at the correct position, see, for example, Figs. 4 and 12 in Ref. [4] or Fig. 4 in Ref. [49]. Most fully-dynamic *r*-process nucleosynthesis calculations within the neutrino-wind model of a core-collapse supernova of type II (SN II) (see, for example, Refs. [50–53]) have confirmed our n_n-T_9 conditions above. For example, Takahashi *et al.* [51] have shown in detail that their time-varying trajectories of neutron densities (or entropies) and temperatures towards freeze-out were exactly lying within our predicted n_n-T_9 band, thus proving the principal validity of our simple and elegant approximation.

The other issues addressed in detail following the above initial results were (i) what additional effects can enter in the ''early'' phases of an *r* process (prior to freeze-out), and (ii) how can an astrophysically realistic treatment of a freeze-out alter the obtained *r*-abundance distribution. A summary of these discussions is given in, for example, the paper of Freiburghaus *et al.* [52]. It was concluded that, while heavy-element production in a realistic astrophysical scenario may well be fast in the very early phase with an *r*-process path close to the neutron drip line, it is the final freeze-out with a path closer to β stability that leaves its fingerprint in the observed $N_{r,\odot}$ pattern. This freeze-out *r*-process path is still 15 to 35 mass units away from β stability. Thus, at freeze-out the *r* process seems to have ''forgotten'' its early history, and nuclear-structure effects of nuclei with $S_n\simeq 1.5$–3 MeV—in particular at the magic neutron shells—determine the final picture. With respect to a realistic treatment of the freeze-out, several effects have been discussed, such as non-equilibrium captures of remaining seed neutrons and their inverse photodisintegrations, recapture of neutrons emitted after β decay, and neutrino reactions [50–69]. The freeze-out tests have, however, shown that these effects do not affect the medium-heavy nuclei up to the $A\simeq 130 N_{r,\odot}$ peak significantly. But—somewhat depending on the specific astrophysical model—they may be important for the heavier nuclides in the rare-earth and the $A\simeq 195 N_{r,\odot}$ regions, although the overall picture will not change.

In summary, we can conclude that despite the above details, our admittedly rather simple and site-independent multicomponent model is a valuable approximation to the still favorably discussed core-collapse SN II scenario, well emulating the conditions just before and at freeze-out. Therefore, the waiting-point approximation has remained an important test bed for systematic parameter studies of various nuclear data sets for masses and β-decay properties [43,67,70–72].

In the context of this paper, the β-decay half-lives of the

TABLE III. Comparison of β-decay half-lives of neutron-magic $N=50$, 82, and 126 *r*-process waiting-point nuclei from different tabulations. In column 2, we list the theoretical $T_{1/2}$ values for pure GT decay [9]. Column 3 summarizes the corresponding values from our new $T_{1/2}$(GT+ff) calculations. And in column 4, we give our experimental values together with the (steadily updated) $T_{1/2}$ evaluation [45,41].

Waiting-point isotope	Beta-decay half-life (ms) $T_{1/2}$ (GT)	$T_{1/2}$ (GT+ff)	$T_{1/2}$ (eval)
^{76}Fe	44.6	27.2	13.2
^{77}Co	13.4	13.7	9.8
^{78}Ni	477.1	224.4	210.0
^{79}Cu	430.3	156.8	188 [a]
^{80}Zn	3068	1260	540 [a]
^{81}Ga	1568	1227	1222 [a]
^{125}Tc	9.1	8.9	7.5
^{126}Ru	34.2	29.7	16.6
^{127}Rh	22.0	20.4	69.7
^{128}Pd	125.1	74.2	115.0
^{129}Ag	47.0	31.7	46 [a]
^{130}Cd	1123.1	502.3	168 [a]
^{131}In	147.1	139.2	278 [a]
^{190}Gd	14.2	9.4	15.8
^{191}Tb	15.9	10.2	13.8
^{192}Dy	31.6	19.7	30.0
^{193}Ho	27.7	17.7	20.4
^{194}Er	87.1	50.2	95.8
^{195}Tm	67.3	42.0	90.4
^{196}Yb	396.6	181.2	222.0

[a]Experimental value.

r-process progenitor isotopes are of major importance since they define to a large extent the time behavior of the *r*-process matter flow from the seed region (here assumed to be Fe) up to the Th, U and the $A \geqslant 250$ fission region. Thus, the half-lives determine the total duration of an *r* process. In particular, the rapidly expanding high-entropy bubble of the neutrino-wind SN II scenario would require a rather short *r*-process time scale of the order of 1 s. Under typical freeze-out conditions ($T_9 \simeq 1.35$ is chosen here) and with an Fe-group seed, this can only be achieved with "short" $T_{1/2}$. This is particularly the case for the classical $N=50$, 82, and 126 waiting-point nuclei where the *r* process *"climbs a staircase with Z and A both increasing by unity after each step"* when plotted versus mass number A [1], or climbs a ladder at the magic shell when plotting versus neutron number N [73,74]. At these magic neutron numbers, the *r*-process isotopes have the longest half-lives (the most important ones at $N \simeq 50$ and 82 have now been determined experimentally, cf. Refs. [21,43,46–48,72,75–77]). Thus, they form the major bottlenecks for the *r*-matter flow at the rising wings of the $N_{r,\odot}$ peaks at $A \simeq 80$, 130, and 195.

Table III compares the $T_{1/2}$(GT) [9] and our new $T_{1/2}$(GT+ff) with the (steadily updated) $T_{1/2}$ evaluation [45,41] used in most of our *r*-process nucleosynthesis calculations since the early 1990's [4]. More than 40 years ago Burbidge *et al.* [1] and Coryell [3] suggested that the sum of the half-lives of all *r*-process isotopes between Fe and the heaviest species in the Th, U region will yield a rough estimate of the total duration of an *r* process (τ_r). When we follow this prescription it immediately becomes evident that our improved macroscopic-microscopic $T_{1/2}$(GT+ff) predictions will speed up the classical *r* process considerably. Within this picture, clearly the $N=50$ shell closure represents the strongest bottleneck for the *r*-matter flow due to the rather long half-lives of ^{80}Zn and ^{81}Ga. Based on the theoretical $T_{1/2}$(GT) from Ref. [9], an *r* process would need about 5.6 s to pass the $N=50$ shell. With our new $T_{1/2}$(GT+ff) values this time would already be reduced to 2.9 s. At the next neutron shell with $N=82$ this value will be within 1.5 s when using the $T_{1/2}$(GT) half-lives, speeded up to 0.8 s with the new $T_{1/2}$(GT+ff) half-lives. The waiting-point ef-

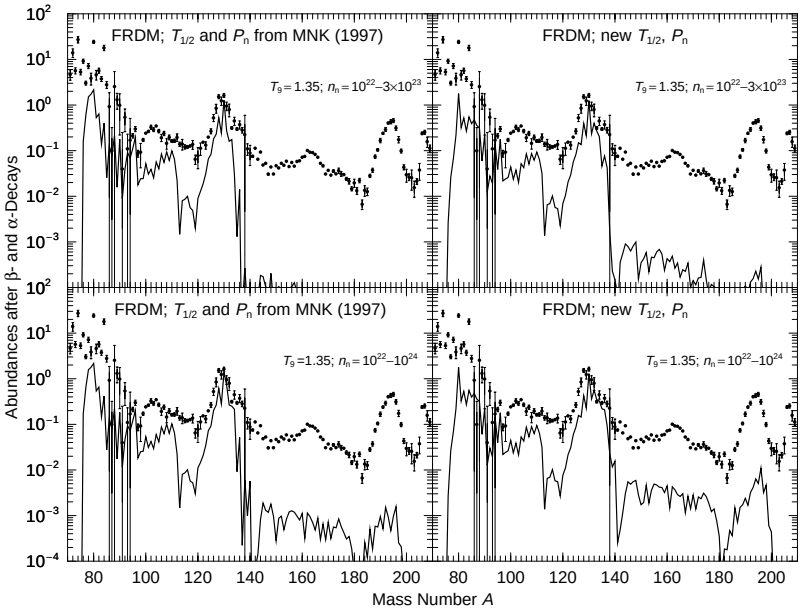

FIG. 11. Comparison of calculated *r*-abundance n_n-τ_r components that mainly build the $A \simeq 130 N_{r,\odot}$ peak at a freeze-out temperature of $T_9=1.35$, using exclusively theoretical $T_{1/2}$(GT) and P_n(GT) values from Ref. [9] (left part) with our new $T_{1/2}$(GT+ff) and P_n(GT+ff) predictions (right part). In all calculations, nuclear masses were used from the Audi evaluation [35] or from the FRDM model [6]. It is clearly evident from this comparison, that—within the same process times $\tau_r=2.00$ s for the upper figures and $\tau_r=2.15$ s for the lower ones—the shorter $T_{1/2}$(GT+ff) result in a faster *r*-matter flow at the $N=82$ bottleneck region, thus producing already considerably higher *r* abundances of rare-earth elements than with the use of the older $T_{1/2}$(GT) values. For more details, see text.

fect is somewhat less pronounced for the $N=126$ shell. When we sum up the theoretical half-lives of the neutron-magic *r*-process nuclei between ^{190}Gd and ^{196}Yb, the use of the $T_{1/2}$(GT) from Ref. [9] yields a value of 0.64 s, to be compared to 0.33 s for the new $T_{1/2}$(GT+ff). In summary, most of the time needed for an *r* process is to overcome the $N=50$ and $N=82$ bottleneck regions, whereas the $N=126$ shell is passed relatively quickly. As soon as the *r* process succeeds in breaking out of the magic neutron shells, the matter flow will accelerate in the regions in between the abundance peaks and beyond $A\simeq 200$. In these regions mainly very short-lived deformed *r*-process progenitors are involved. For these the earlier $T_{1/2}$(GT) [9] are quite similar to our new $T_{1/2}$(GT+ff) predictions.

Today we know, however, that the initial picture of Burbidge *et al.* [1] of summing-up the $T_{1/2}$ of the waiting-point nuclei is too simplistic, and in fact not quite correct. Since the early 1990's, at the latest, when the first experimental information about the *r*-process isotopes ^{80}Zn and ^{130}Cd became available, it is definitely clear that the formation of the three $N_{r,\odot}$ peaks requires different neutron-density conditions, implying different *r*-process paths at different distances from β stability [4,70,74]. To be more specific, under the astrophysical $n_{\rm n}$-$\tau_{\rm r}$ conditions where the $A\simeq 80$ peak is produced at relatively ''low'' $n_{\rm n}$, the $A\simeq 130$ peak will only barely be formed and the $A\simeq 195$ peak not at all, unless ''higher'' $n_{\rm n}$ densities are invoked. For other $n_{\rm n}$-τ_r conditions where the $A\simeq 130$ peak is produced at ''medium'' $n_{\rm n}$ densities (see, e.g., Fig. 11 of this paper), the $A\simeq 80$ region has already been partly depleted, and the $A\simeq 195$ peak only starts to fill up.

To show the situation in more detail, Fig. 11 compares snapshots of *r*-abundance calculations for a range of astrophysical conditions (with identical T_9, $n_{\rm n}$, and τ_r, respectively) under which the second $N_{r,\odot}$ peak at $A\simeq 130$ is formed. Together with the neutron separation energies from the FRDM mass model [6], the $T_{1/2}$ and $P_{\rm n}$ values become the decisive nuclear quantities in these calculations. And, as is clearly evident from the figure, with our new, ''shorter'' $T_{1/2}$(GT+ff) and the same process time considerably more *r* material has been built up beyond the peak in the rare-earth region than with our old, ''longer'' $T_{1/2}$(GT).

Finally, Fig. 12 shows the development of the *r* abundances of the important waiting-point isotopes ^{80}Zn ($N=50$), ^{130}Cd ($N=82$), and ^{195}Tm ($N=126$) as a function of neutron density $n_{\rm n}$ and process duration τ_r, respectively. These three nuclei form the respective tops of the three $N_{r,\odot}$ peaks at freeze-out prior to β-decay back to stability. Again, one observes that the new macroscopic-microscopic $T_{1/2}$(GT+ff) predictions result in a speeding-up of the *r* process compared to the earlier half-lives for pure GT decay [9]. Under these conditions the total duration for a robust *r*-process nucleosynthesis up to Th, U is reduced to about 4 s.

In this paper, we have for consistency reasons based all our calculations on the FRDM mass model [6], in which neutron-shell corrections in the vicinity of magic neutron numbers far from stability, in particular in the waiting-point

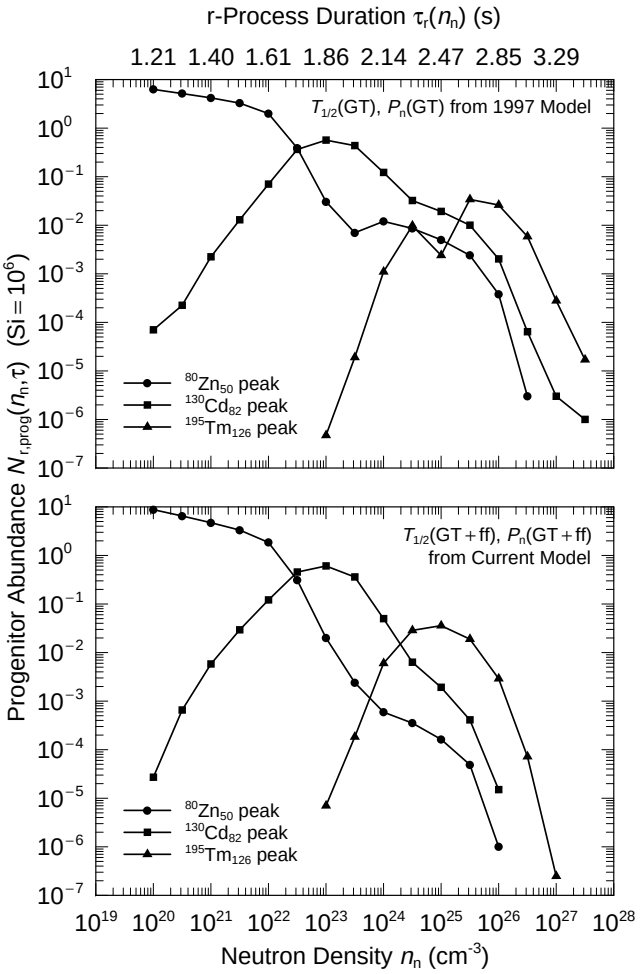

FIG. 12. The buildup of the initial *r* abundances $N_{r,\rm prog}$ of the three neutron-magic waiting-point nuclides ^{80}Zn$_{50}$, ^{130}Cd$_{82}$, and ^{195}Tm$_{126}$ from an Fe seed as a function of neutron density $n_{\rm n}$ and process duration τ_r at freeze-out temperature $T_9=1.35$. The above three isotopes are the direct progenitors of the stable isobars ^{80}Se, ^{130}Te, and ^{195}Pt situated at the top of the respective $N_{r,\odot}$ peaks. Their buildup contains the full time history of the *r* process ''climbing up'' the respective magic neutron shells at $N=50$, 82, and 126. Furthermore, in the formation of the second and third $N_{r,\odot}$ peaks, a kind of ''memory effect'' of the history of the *r*-matter flow at the earlier *r* peak(s) is maintained. The upper part shows the calculations using the β-decay half-lives $T_{1/2}$(GT) obtained from the QRPA model for GT decay only [8]. The lower part exhibits the respective calculations using our new, shorter theoretical $T_{1/2}$(GT+ff) values that include both GT decay (from the QRPA model) and ff-decay (from the ''gross theory'' [25]). In all calculations, nuclear masses have consistently been taken from the Audi 1995 evaluation [35] and from the FRDM model [6].

regions, are sometimes as strong as the experimentally known ones in the valley of β stability. This model currently presents the most well tested and most unified prescription for obtaining unknown nuclear properties far from stability, with the best proven overall track record of reliability for a large number of nuclear-structure properties, when calculated quantities are compared to new data as they become available [9]. However, it is informative to investigate the conse-

quences of the recent experimental evidence of a gradual shell weakening (''quenching'') of the classical shell gaps with distance from stability. This feature—already well known for $N=20$ and $N=28$—also seems to occur at $N=50$ and $N=82$. For recent reviews, see, for example, Refs. [43,72]. Such a weakening of the shell effects may further speed up the classical *r* process even at moderate neutron densities. In a calculation based on, for example, the microscopic HFB method with the specific Skyrme force SkP of Dobaczewski *et al.* [78,79], which exhibits a rather strong shell quenching, a robust process from the classical Fe seed up to the full third $N_{r,\odot}$ peak could be run within about 1.5 s with a maximum neutron density of only $n_n \simeq 10^{23}$ (cm^{-3}) (see, e.g., Fig. 3 in Ref. [70] or Fig. 4 in Ref. [72]).

However, in, for example, the neutrino-wind SN II scenario, the rapid-neutron-capture process starts from an $A \simeq 90$ seed composition, and consequently it avoids the dominant $N=50$ bottleneck in the *r*-matter flow. In this scenario, with a calculation based on the ''quenched-shell'' mass models, such as the ETFSI-*Q* [12] model, the total duration of an *r* process at freeze-out can be further reduced to about 850 ms. In this calculation we used the ETFSI-*Q* masses to determine all mass-related quantities, for example, the Q_β values that were used in the calculation of the $T_{1/2}(\mathrm{GT+ff})$.

It will presumably not be a problem to obtain short half-lives of *r*-process progenitor nuclei and corresponding short time scales to build up heavy elements in low-entropy environments which are very neutron rich, such as neutron-star mergers [80–82], but it is still a difficult problem to realize short progenitor half-lives in high-entropy environments with (only) moderate neutron densities, such as SN II scenarios. As shown by, for example, Refs. [50–52,57,64], rather high entropies up to 400 k_B/nucleon are required to produce the full third $N_{r,\odot}$ peak at $A \simeq 195$. Such high entropies, corresponding to high densities are considerably beyond what is achieved in realistic hydrodynamic approaches. However, if shell quenching at $N=50$ and 82 would definitely be confirmed by future experiments, the above maximum neutron density of roughly 10^{23} (cm^{-3})—which would correspond to a maximum entropy of about 150 k_B/nucleon—together with an *r*-process time scale of the order of 1 s might help to solve at least some of the still existing problems encountered in the high-entropy neutrino-wind SN II scenario.

V. SUMMARY AND CONCLUSIONS

We have combined our microscopic QRPA model of allowed Gamow-Teller β decay with the statistical gross theory of first-forbidden decay. Experimental data show that the first-forbidden strength over a given energy range is represented by numerous densely spaced peaks whereas the allowed GT strength is concentrated in a few strong peaks. Our new ''microscopic-macroscopic'' model of β decay is therefore a reasonable approximation in analogy with the microscopic-macroscopic model of nuclear potential-energy surfaces. Also, it is currently the only tractable way to globally calculate the required nuclear structure and decay properties in a model that represents a unified, nondivergent approach across the entire nuclear chart. The model has a proven track record of reliability when it is applied far from known regions of nuclei where the model parameters were determined [6,9]. We have tested our calculations by comparing the new model and old model, the latter without first-forbidden decays taken into account, to data throughout the periodic system. These comparisons demonstrated that our enhanced model leads to a substantial improvement in calculated β-decay half-lives and β-delayed neutron-emission probabilities. This is particularly true near magic neutron numbers where the *r* process ''spends most of its time.''

The new $T_{1/2}(\mathrm{GT+ff})$ and $P_n(\mathrm{GT+ff})$ values have been applied to site-independent *r*-process calculations. Calculations based on the new data base result in a considerable speeding-up of the *r*-matter flow in the vicinity of the $N_{r,\odot}$ peaks, which are related to magic neutron-shell closures, relative to calculations based on the previous $T_{1/2}(\mathrm{GT})$ and $P_n(\mathrm{GT})$ tabulation.

Clearly, still more work is needed in both experimental and theoretical nuclear physics as well as in astrophysics to finally solve the problem of the *"origin of the heavy elements between Fe and Th, U"* which has recently been considered number three among: ''The 11 Greatest Unanswered Questions in Physics'' [83].

ACKNOWLEDGMENTS

This work was supported by the U.S. Department of Energy, the German Bundesministerium für Bildung und Forschung, and Gesellschaft für Schwerionenforschung.

[1] E.M. Burbidge, G.R. Burbidge, W.A. Fowler, and F. Hoyle, Rev. Mod. Phys. **29**, 547 (1957).
[2] A. G. W. Cameron, Atomic Energy of Canada Report No. CRL-41, 1957.
[3] C.D. Coryell, J. Chem. Educ. **38**, 67 (1961).
[4] K.-L. Kratz, J.-P. Bitouzet, F.-K. Thielemann, P. Möller, and B. Pfeiffer, Astrophys. J. **403**, 216 (1993).
[5] P. Möller and J.R. Nix, At. Data Nucl. Data Tables **26**, 165 (1981).
[6] P. Möller, J.R. Nix, W.D. Myers, and W.J. Swiatecki, At. Data Nucl. Data Tables **59**, 185 (1995).
[7] J. Krumlinde and P. Möller, Nucl. Phys. **A417**, 419 (1984).
[8] P. Möller and J. Randrup, Nucl. Phys. **A514**, 1 (1990).
[9] P. Möller, J.R. Nix, and K.-L. Kratz, At. Data Nucl. Data Tables **66**, 131 (1997).
[10] P.A. Seeger and W.M. Howard, Nucl. Phys. **A238**, 491 (1975).
[11] Y. Aboussir, J.M. Pearson, A.K. Dutta, and F. Tondeur, At. Data Nucl. Data Tables **61**, 127 (1995).
[12] J.M. Pearson, R.C. Nayak, and S. Goriely, Phys. Lett. B **387**, 455 (1996); (private communication).

[13] S. Goriely, F. Tondeur, and J.M. Pearson, At. Data Nucl. Data Tables **77**, 311 (2001).
[14] O. Bohigas and P. Lebœuf, Phys. Rev. Lett. **88**, 2502 (2002).
[15] O. Bohigas and P. Lebœuf, Phys. Rev. Lett. **88**, 9903 (2002).
[16] C.L. Duke, P.G. Hansen, O.B. Nielsen, and G. Rudstam, Nucl. Phys. **A151**, 609 (1970).
[17] T. Tachibana, H. Nakata, and M. Yamada, in *Tours Symposium on Nuclear Physics III*, edited by M. Arnould, M. Lewitowicz, Yu. Ts. Oganessian, M. Ohta, H. Utsunomiya, and T. Wada, AIP Conf. Proc. No. 425 (AIP, Woodbury, NY, 1998), p. 495.
[18] K.-L. Kratz, Nucl. Phys. **A417**, 447 (1984).
[19] O. Sorlin, D. Guillemaud-Mueller, A.C. Müller, V. Borrel, S. Dogny, F. Pougheon, K.-L. Kratz, H. Gabelmann, B. Pfeiffer, A. Wöhr, W. Ziegert, Y.E. Penionzhkevich, S.M. Lukyanov, V.S. Salamatin, R. Anne, C. Borcea, L.K. Fifield, M. Lewitowicz, M.G. Saint-Laurent, D. Bazin, C. Détraz, F.-K. Thielemann, and W. Hillebrandt, Phys. Rev. C **47**, 2941 (1993).
[20] K.-L. Kratz, P. Möller, and W.B. Walters, in *Capture Gamma-Ray Spectroscopy and Related Topics*, edited by Stephen Wender, AIP Conf. Proc. No. 529 (AIP, Melville, NY, 2000), p. 295.
[21] M. Hannawald, K.L. Kratz, B. Pfeiffer, W.B. Walters, V.N. Fedoseyev, V.I. Mishin, W.F. Mueller, H. Schatz, J. VanRoosbroeck, U. Köster, V. Sebastian, and H.L. Ravn, Phys. Rev. C **62**, 4301 (2000).
[22] A. Wöhr, A. Ostrowski, K.-L. Kratz, I. Dillmann, A. M. El-Taher, V. Fedoseyev, L. Fraile, H. Fynbö, U. Köster, B. Pfeiffer, H. L. Ravn, M. Seliverstov, J. Shergur, L. Weissman, W. B. Walters, and the ISOLDE Collaboration, in *Proceedings of the 11th Workshop on Nuclear Astrophysics*, Ringberg Castle, Lake Tegernsee, Germany, 2002, edited by W. Hillebrandt and E. Müller (MPI fur Astrophysik, Garching, 2002), Max-Planck-Institut für Astrophysik Report No. MPA/P13, 2002, p. 79.
[23] K.-L. Kratz and G. Herrmann, Z. Phys. **263**, 435 (1973).
[24] K. Takahashi, Prog. Theor. Phys. **47**, 1500 (1972).
[25] K. Takahashi, M. Yamada, and T. Kondoh, At. Data Nucl. Data Tables **12**, 101 (1973).
[26] I.N. Borzov, S.A. Fayans, E. Kromer, and D. Zawischa, Z. Phys. A **355**, 117 (1996).
[27] M. Hirsch, A. Staudt, K. Muto, and H.V. Klapdor-Kleingrothaus, At. Data Nucl. Data Tables **53**, 165 (1993).
[28] I. Hamamoto, Nucl. Phys. **62**, 49 (1965).
[29] J.A. Halbleib, Sr., and R.A. Sorensen, Nucl. Phys. **A98**, 542 (1967).
[30] J. Randrup, Nucl. Phys. **A207**, 209 (1973).
[31] M. A. Preston, *Physics of the Nucleus* (Addison-Wesley, Reading, 1962).
[32] N.B. Gove and M.J. Martin, Nucl. Data Tables **10**, 205 (1971).
[33] A. deShalit and H. Feshbach, *Theoretical Physics*, Nuclear Structure Vol. I (Wiley, New York, 1974).
[34] G. Audi (private communication), with four revisions.
[35] G. Audi and A.H. Wapstra, Nucl. Phys. **A595**, 409 (1995).
[36] K.-L. Kratz, H. Ohm, K. Sümmerer, M. Zendel, G. Jung, K.D. Wünsch, C. Ristori, J. Crancon, and S.G. Prussin, Phys. Lett. **86B**, 21 (1979).
[37] K.-L. Kratz, H. Ohm, A. Schroeder, H. Gabelmann, W. Ziegert, H.V. Klapdor, J. Metzinger, T. Oda, B. Pfeiffer, G. Jung, L. Alquist, and G. I. Crawford, in *Proceedings of the 4th International Conference on Nuclei far from Stability*, Helsingør, 1981, edited by P. G. Hansen and D. B. Nielsen, CERN-Report No. 81-09, p. 317.
[38] H. Franz, J.V. Kratz, K.-L. Kratz, W. Rudolph, G. Herrmann, F.M. Nuh, S.G. Prussin, and A.A. Shihab-Eldin, Phys. Rev. Lett. **33**, 859 (1974).
[39] K.-L. Kratz, W. Rudolph, H. Ohm, H. Franz, M. Zendel, G. Herrnann, S.G. Prussin, F.M. Nuh, A.A. Shihab-Eldin, D.R. Slaughter, W. Halverson, and H.V. Klapdor, Nucl. Phys. **A317**, 311 (1979).
[40] S. Raman, B. Fogelberg, J.A. Harvey, R.L. Macklin, P.H. Stelson, A. Schröder, and K.-L. Kratz, Phys. Rev. C **28**, 602 (1983).
[41] B. Pfeiffer, K.-L. Kratz, and P. Möller, Prog. Nucl. Energy **41/1–4**, 39 (2002).
[42] URL: http://t16web/Moller/publications/rspeed2002.html
[43] K.-L. Kratz, B. Pfeiffer, F.-K. Thielemann, and W.B. Walters, Hyperfine Interact. **129**, 185 (2000).
[44] K.-L. Kratz, P. Möller, B. Pfeiffer, and F.-K. Thielemann, in *Proceedings of 8th International Symposium on Capture Gamma-ray Spectroscopy and Related Topics*, Fribourg, 1993, edited by J. Kern (World Scientific, Singapore, 1994), p. 724.
[45] K.-L. Kratz, B. Pfeiffer, and P. Möller, KCh Mainz Report, 1996 (unpublished) and URL: www.kernchemie.uni-mainz.de/~pfeiffer/khf/
[46] K.-L. Kratz, H. Gabelmann, W. Hillebrandt, B. Pfeiffer, K. Schlosser, and F.-K. Thielemann, Z. Phys. **385**, 489 (1986).
[47] B. Ekström, B. Fogelberg, P. Hoff, E. Lund, and A. Sangariyavanish, Phys. Scr. **34**, 614 (1986).
[48] R.L. Gill, R.F. Casten, D.D. Warner, A. Piotrowski, H. Mach, J.C. Hill, F.K. Wohn, J.A. Winger, and R. Moreh, Phys. Rev. Lett. **56**, 1874 (1986).
[49] K.-L. Kratz *et al.*, *Origin of the Elements in the Solar System: Implications of Post-1957 Observations* (Kluwer/Plenum, New York, 2001), p. 119.
[50] B.S. Meyer, G.J. Mathews, W.M. Howard, S.E. Woosley, and R.D. Hoffman, Astrophys. J. **399**, 656 (1992).
[51] K. Takahashi, J. Witti, and H.-T. Janka, Astron. Astrophys. **286**, 857 (1994).
[52] C. Freiburghaus, J.F. Rembges, T. Rauscher, E. Kolbe, F.-K. Thielemann, K.-L. Kratz, B. Pfeiffer, and J.J. Cowan, Astrophys. J. **516**, 381 (1999).
[53] C. Freiburghaus, S. Rosswog, and F.-K. Thielemann, Astrophys. J. Lett. **525**, L121 (1999).
[54] F.-K. Thielemann, A. G. W. Cameron, and J. J. Cowan, in *Proceedings of 50 Years with Nuclear Fission*, Gaithersburg, 1989, edited by J. W. Behrens and A. D. Carlson (American Nuclear Society, La Grange Park, 1989), p. 592.
[55] B.S. Meyer, Astrophys. J. **343**, 254 (1989).
[56] J.J. Cowan, F.-K. Thielemann, and J.W. Truran, Phys. Rep. **208**, 267 (1991).
[57] Y.Z. Qian and S.E. Woosley, Astrophys. J. **471**, 331 (1996).
[58] E. Kolbe, K. Langanke, and F.-K. Thielemann, Eur. Phys. J. A **3**, 389 (1998).
[59] A. Hektor, E. Kolbe, K. Langanke, and J. Toivanen, Phys. Rev. C **61**, 5803 (2000).
[60] G.M. Fuller and B.S. Meyer, Astrophys. J. **453**, 792 (1995).
[61] G.C. McLaughlin and G.M. Fuller, Astrophys. J. Lett. **464**, L143 (1996).

[62] Y.-Z. Qian, P. Vogel, and G.J. Wasserburg, Astrophys. J. **494**, 285 (1998).
[63] B.S. Meyer, G.C. McLaughlin, and G.M. Fuller, Phys. Rev. C **58**, 3696 (1998).
[64] S.E. Woosley, J.R. Wilson, G.J. Mathews, R.D. Hoffman, and B.S. Meyer, Astrophys. J. **433**, 229 (1994).
[65] R.D. Hoffman, S.E. Woosley, and Y.-Z. Qian, Astrophys. J. **482**, 951 (1997).
[66] K. Langanke and E. Kolbe, At. Data Nucl. Data Tables **79**, 293 (2001).
[67] K.-L. Kratz, Nucl. Phys. **A688**, 308c (2001).
[68] Y.-Z. Qian, W.C. Haxton, K. Langanke, and P. Vogel, Phys. Rev. C **55**, 1532 (1997).
[69] K. Langanke and G. Martinez-Pinedo, Rev. Mod. Phys. (unpublished).
[70] K.-L. Kratz, B. Pfeiffer, and F.-K. Thielemann, Nucl. Phys. **A630**, 352c (1998).
[71] B. Pfeiffer, K.-L. Kratz, and F.-K. Thielemann, Z. Phys. A **357**, 235 (1997).
[72] B. Pfeiffer, K.-L. Kratz, F.-K. Thielemann, and W.B. Walters, Nucl. Phys. **A693**, 282 (2001).
[73] K.-L. Kratz, F.-K. Thielemann, W. Hillebrandt, P. Möller, V. Harms, A. Wöhr, and J. W. Truran, in *Proceedings of 6th International Symposium on Capture Gamma-ray Spectroscopy, 1987*, edited by K. Abrahams and P. Van Asche, IOP Conf. Proc. No. 88 [J. Phys. G **14**, S331 (1988)].
[74] K.-L. Kratz, Rev. Mod. Astron. **1**, 184 (1988).
[75] K.-L. Kratz, H. Gabelmann, P. Möller, B. Pfeiffer, H. L Ravn, and A. Wöhr, Z. Phys. A **340**, 419 (1994).
[76] K.-L. Kratz, T. Kautzsch, M. Hannawald, W. Böhmer, I. Klöckl, P. Möller, B. Pfeiffer, V.N. Fedoseyev, V.I. Mishin, W.B. Walters, A. Wöhr, P. van Duppen, Y. Jading, H. L. Ravn, J. Lettry, V. Sebastian, M. Koizumi, U. Köster, and the ISOLDE Collaboration, in *Proceedings of International Conference on Fission and Properties of Neutron-Rich Nuclei*, Sanibel Island, Florida, 1997, edited by J. H. Hamilton and A. V. Ramayya (World Scientific, Singapore, 1998), p. 586.
[77] K.-L. Kratz, in *ENAM 98, Exotic Nuclei and Atomic Masses*, edited by Bradley M. Sherrill, David J. Morrissey, and Cary N. Davids, AIP Conf. Proc. No. 455 (AIP, Woodbury, NY, 1998), p. 827.
[78] J. Dobaczewski, I. Hamamoto, W. Nazarewicz, and J.A. Sheikh, Phys. Rev. Lett. **72**, 981 (1994).
[79] J. Dobaczewski, W. Nazarewicz, and T.R. Werner, Phys. Scr., T **56**, 15 (1995).
[80] J.M. Lattimer, F. Mackie, D.G. Ravenhall, and D.N. Schramm, Astrophys. J. **213**, 225 (1977).
[81] S. Rosswog, M. Liebendorfer, F.-K. Thielemann, M.B. Davies, W. Benz, and T. Piran, Astron. Astrophys. **341**, 499 (1999).
[82] S. Rosswog, M.B. Davies, F.-K. Thielemann, and T. Piran, Astron. Astrophys. **360**, 171 (2000).
[83] E. Haseltine, Discover Magazine, Vol. 23, No. 2, February 2002.